Stability Analysis of DFIG System connected with High-Frequency Capacitive Grid based on Closed-Loop Current Control and Direct Power Control

Bin Hu[1], Heng Nian[1], Subham Sahoo[2], Frede Blaabjerg[2], Yaqian Zhang[3], Zixiao Xu[4]

[1]College of Electrical Engineering
Zhejiang University
Hangzhou, China
11810031@zju.edu.cn
nianheng@zju.edu.cn

[3]College of Electrical Engineering
Southeast University
Nanjing, China
yaqianzhang83@seu.edu.cn

[2]Department of Energy Technology
Aalborg University
Aalborg, Denmark
sssa@energy.aau.dk
fbl@energy.aau.dk

[4]Department of Electrical Engineering
Northwestern Polytechnical University
Xi'an, China
xuzixiao_9602@mail.nwpu.edu.cn

Acknowledgements

This work was supported by the National Natural Science Foundation of China under Grant 51977194.

Keywords

«Impedance analysis», «Coupling characteristics», «Direct power control», «Doubly-Fed Induction Generator», «Stability analysis»

Abstract

This paper analyzes the stability of doubly-fed induction generator (DFIG) system connected with high-frequency capacitive grid based on closed-loop current control (CCC) and direct power control (DPC). There will be some high-frequency resonance issues when employs DPC. Consequently, the reason of this high-frequency resonance and frequency coupling characteristic are studied.

Introduction

Doubly-fed induction generator (DFIG) has the advantages of low cost, small converter rating, competitive durability and flexible power adjustment capability, which is popular for the commercial wind power generation system around the globe [1], [2]. Nowadays, the grid network has been more complex due to the diversified equipment, such as parallel compensation, long transmission cable, high voltage DC (HVDC), and STATCOM [3]. It is widely adopted that the interconnected grid with DFIG will change from inductive grid to high-frequency capacitive grid [3]. An impedance sweeping test has been employed in the AC network of the Guangxi-side of Luxi district in China. It can be found that the AC grid behaves as a capacitance at high frequency, and the cut-off frequency is 866 Hz [4].

Closed-loop current control (CCC) and direct power control (DPC) are two common control strategies for DFIG system [5]. Compared with CCC, the DPC can directly control the active power and reactive power, which can enhance the power dynamic response [6]. Furthermore, Ohnishi proposed a simple structure of DPC combining the instantaneous power theory and direct torque control [7]. This DPC is based on the PWM modulation without the selection of single voltage vector and the application of hysteresis controller [8], [9].

This paper obtains an interesting phenomenon, where DFIG system based on CCC is always stable under the high-frequency capacitive grid, while the DFIG system based on DPC has some resonance

issues. And there will be high-frequency coupling characteristics during the high-frequency oscillation of DFIG system. However, the DFIG system based on CCC may behave as a passivity inductance at high frequency, which is often misinterpreted as the origin of high-frequency resonance and high-frequency coupling characteristics.

Topology of DFIG system connected with high-frequency capacitive grid

The investigated configuration diagram of DFIG system is depicted in Fig. 1. The control signals of DFIG system are generated from the rotor side converter (RSC) and grid side converter (GSC). Normally, the GSC can keep the stable dc voltage for DFIG system, and the RSC can achieve the maximum power tracking (MPPT) and provide the maximum expected active power.

Except the inductive weak grid, there are two common configurations of weak networks to satisfy the requirement of power quality compensation and long-distance transmission: 1) parallel compensated network with grid inductance L_g and compensated capacitance C_{com}; 2) long transmission cable modelled as the series connection of several Π units with the cable resistor R_1, the cable inductor L_1 and the cable shunt capacitor $C_1/2$.

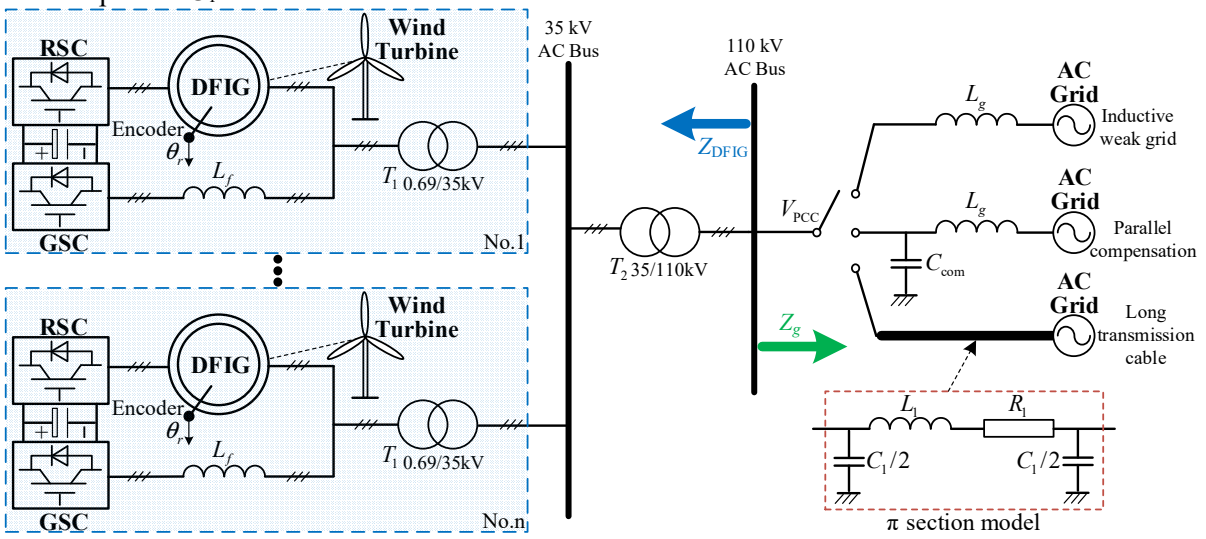

Fig. 1: Investigated configuration diagram of DFIG system

Compared with the inductive weak grid, the parallel compensated network and long transmission cable contain the parallel capacitance, which always present capacitive at high frequency. An impedance sweeping test has been employed in the AC network of the Guangxi-side of Luxi district in China. It can be found that the AC grid can be equivalent to the high-frequency capacitive grid in Fig. 2 with the cut-off frequency of 866 Hz [4]. To be honest, it is more reasonable to model the long transmission cable with multiple Π units. However, this paper pays more attention to the stability issues of different control strategies when there is a parallel capacitor in the weak grid, so the long transmission cable is also regarded as a high-frequency capacitive grid for simplify.

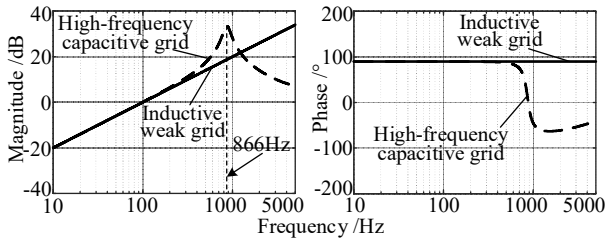

Fig. 2: Bode diagram of inductive weak grid and high-frequency capacitive grid

Fig. 3 depicts the simplified topology of DFIG system connected with high-frequency capacitive grid. According to Fig. 3, the DFIG system is connected to a high-frequency capacitive grid, such that

the additional resistor R_g and capacitance C_g will be parallel with the grid inductance L_g. The other parameters of DFIG system is shown in Table I.

Table I: Parameters of DFIG system

Symb	Parameter	Value
U_s	Rated voltage	690 V
P_s	Rated power	1.5 MW
f_1	Fundamental frequency	50 Hz
f_r	Rotor frequency	35 Hz
n_p	Pole pairs	2
V_{dc}	Dc-link voltage	1050 V
L_{ls}	Stator leakage	0.06 mH
L_{lr}	Rotor leakage	0.083 mH
L_m	Mutual inductance	4.43 mH
R_s	Stator resistance	2.4 mΩ
R_r	Rotor resistance	2 mΩ
K_e	Turns ratio	0.33
f_s	Switching frequency	5 kHz

The GSC is ignored in this paper and the dc-link voltage V_{dc} is assumed to be constant, the reason is as follow: 1) The overall impedance of DFIG system can be equal to the parallel connection of DFIG+RSC and GSC, but the one with larger magnitude will play a leading role; 2) the magnitude of impedance is related to the output power under the same port voltage, while the GSC can only output the limited slip power; 3) there is a L or LCL type filter between the point of common coupling (PCC) and the GSC, which further increase the magnitude of GSC.

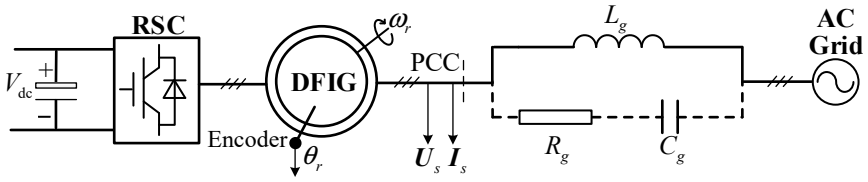

Fig. 3: Simplified topology of DFIG system connected with high-frequency capacitive grid

High-frequency resonance issues when switching from CCC to DPC

The resonance issues of DFIG system based on DPC connected with high-frequency capacitive grid is shown in Fig. 4. When switched from DPC to CCC, the resonance issues can be suppressed. Fig. 5 is the FFT analysis, it can be found that this high-frequency resonance issues have a frequency coupling characteristics, indicating that there will be two frequencies differing by 100 Hz in the spectrum together. However, the frequency coupling always exist in an asymmetrical way in the controller. It is worth notifying that the influence of controller has been ignored due to the limited bandwidth. In addition, when the proportional integral (PI) parameter of DPC controller is increased, there will be multiple coupling frequencies.

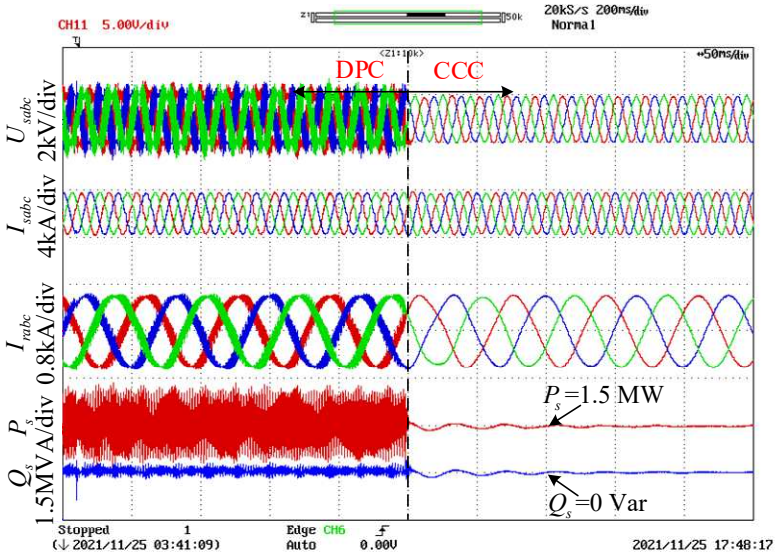

Fig. 4: Resonance issues of DFIG system based on DPC connected with high-frequency capacitive grid

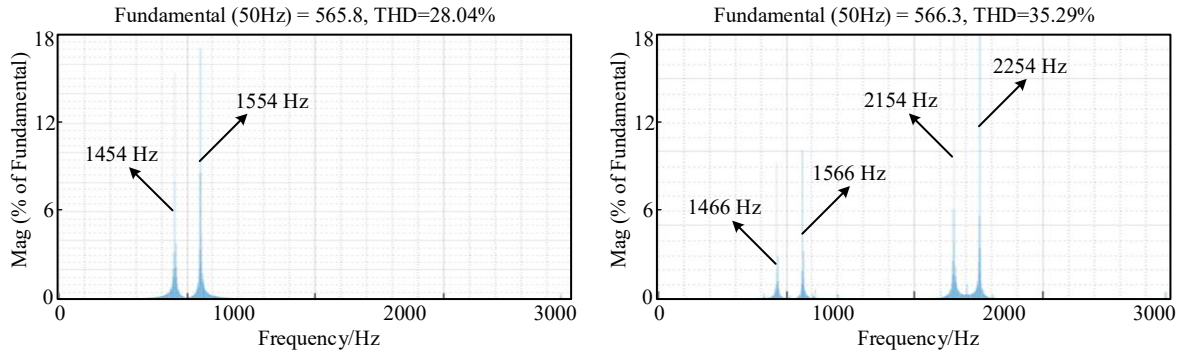

(a) K_p=0.6 K_i=60 (b) K_p=0.8 K_i=80

Fig. 5: FFT analysis of DFIG system based on DPC connected with high-frequency capacitive grid

Impedance modeling and analysis of Nyquist diagram

This paper establishes the impedance model of DFIG system based on CCC and DPC as shown in Fig. 6. And Fig. 7 depicts the Nyquist diagram for the developed impedance model.

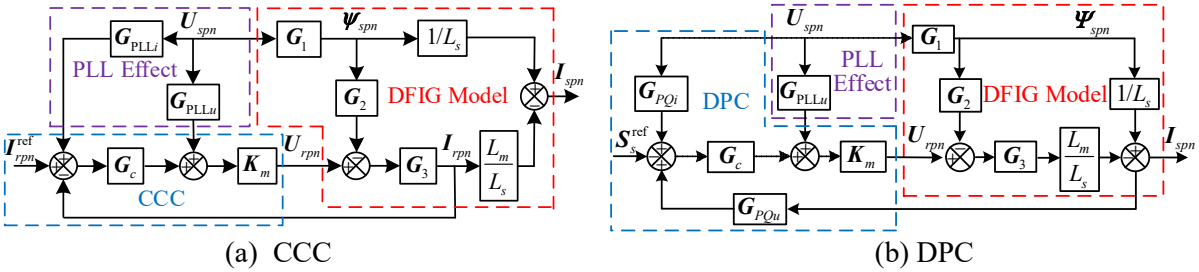

(a) CCC (b) DPC

Fig. 6: Impedance model of DFIG system based on CCC and DPC

$$\boldsymbol{G}_1=\begin{bmatrix}\dfrac{1}{s} & 0\\ 0 & \dfrac{1}{s-2\mathrm{j}\omega_g}\end{bmatrix}\quad \boldsymbol{G}_2=\frac{L_m}{L_s}\begin{bmatrix}s-\mathrm{j}\omega_r & 0\\ 0 & s+\mathrm{j}\omega_r-2\mathrm{j}\omega_g\end{bmatrix}$$

$$\boldsymbol{G}_3=\begin{bmatrix}\dfrac{1}{R_r+(s-\mathrm{j}\omega_r)L_r\sigma} & 0\\ 0 & \dfrac{1}{R_r+(s+\mathrm{j}\omega_r-2\mathrm{j}\omega_g)L_r\sigma}\end{bmatrix} \tag{1}$$

$$\boldsymbol{G}_c=\begin{bmatrix}\dfrac{K_{pc}(s-\mathrm{j}\omega_g)+K_{ic}}{s-\mathrm{j}\omega_g} & 0\\ 0 & \dfrac{K_{pc}(s-\mathrm{j}\omega_g)+K_{ic}}{s-\mathrm{j}\omega_g}\end{bmatrix} \tag{2}$$

$$\boldsymbol{K}_m=\begin{bmatrix}e^{-1.5s/f_s} & 0\\ 0 & e^{-1.5(s-2\mathrm{j}\omega_g)/f_s}\end{bmatrix} \tag{3}$$

$$\boldsymbol{G}_{\mathrm{PLL}i}=\frac{1}{2}\begin{bmatrix}-\boldsymbol{I}_{rdq0}H_{\mathrm{PLL}}(s) & \boldsymbol{I}_{rdq0}H_{\mathrm{PLL}}(s)\\ \boldsymbol{I}^*_{rdq0}H_{\mathrm{PLL}}(s) & -\boldsymbol{I}^*_{rdq0}H_{\mathrm{PLL}}(s)\end{bmatrix}\quad \boldsymbol{G}_{\mathrm{PLL}u}=\frac{1}{2}\begin{bmatrix}\boldsymbol{U}_{rdq0}H_{\mathrm{PLL}}(s) & -\boldsymbol{U}_{rdq0}H_{\mathrm{PLL}}(s)\\ -\boldsymbol{U}^*_{rdq0}H_{\mathrm{PLL}}(s) & \boldsymbol{U}^*_{rdq0}H_{\mathrm{PLL}}(s)\end{bmatrix} \tag{4}$$

$$\boldsymbol{G}_{PQu}=\begin{bmatrix}\boldsymbol{U}_{sdq0} & 0\\ 0 & \boldsymbol{U}^*_{sdq0}\end{bmatrix}\quad \boldsymbol{G}_{PQi}=\begin{bmatrix}0 & \boldsymbol{I}_{sdq0}\\ \boldsymbol{I}^*_{sdq0} & 0\end{bmatrix} \tag{5}$$

where the $\boldsymbol{G}_1$, $\boldsymbol{G}_2$ and $\boldsymbol{G}_3$ are the DFIG parameter matrices. $\boldsymbol{G}_c$ is the current controller matrix, that K_{pc} and K_{ic} are the proportional gain and integral gain of current controller. $\boldsymbol{K}_m$ is the system delay matrix. $\boldsymbol{G}_{\mathrm{PLL}i}$ and $\boldsymbol{G}_{\mathrm{PLL}u}$ are the PLL matrices related to the rotor current coordinate transformation and rotor voltage coordinate transformation. $\boldsymbol{G}_{\mathrm{PLL}i}$ and $\boldsymbol{G}_{\mathrm{PLL}u}$ are the power calculation matrices. The subscripts p and n denote the positive and negative sequence components. The superscript ref is the reference value. * represents the conjugate operator. The subscript 0 denotes the steady-state component. $H_{\mathrm{PLL}}(\mathrm{s})=H_p(\mathrm{s})/[U_{sd0}H_p(\mathrm{s})+s\text{-}\mathrm{j}\omega_g]$. The PI controller of the PLL is denoted as $H_p(s)=K_{pp}+K_{ip}/(s\text{-}\mathrm{j}\omega_g)$, in which K_{pp} and K_{ip} are the proportional gain and integral gain of PLL. K_{pc} and K_{ic} are the proportional gain and integral gain of current or power controller. ω_g is the grid angular frequency, and ω_r is the rotor angular frequency. $\sigma=1\text{-}L_m^2/(L_s\cdot L_r)$.

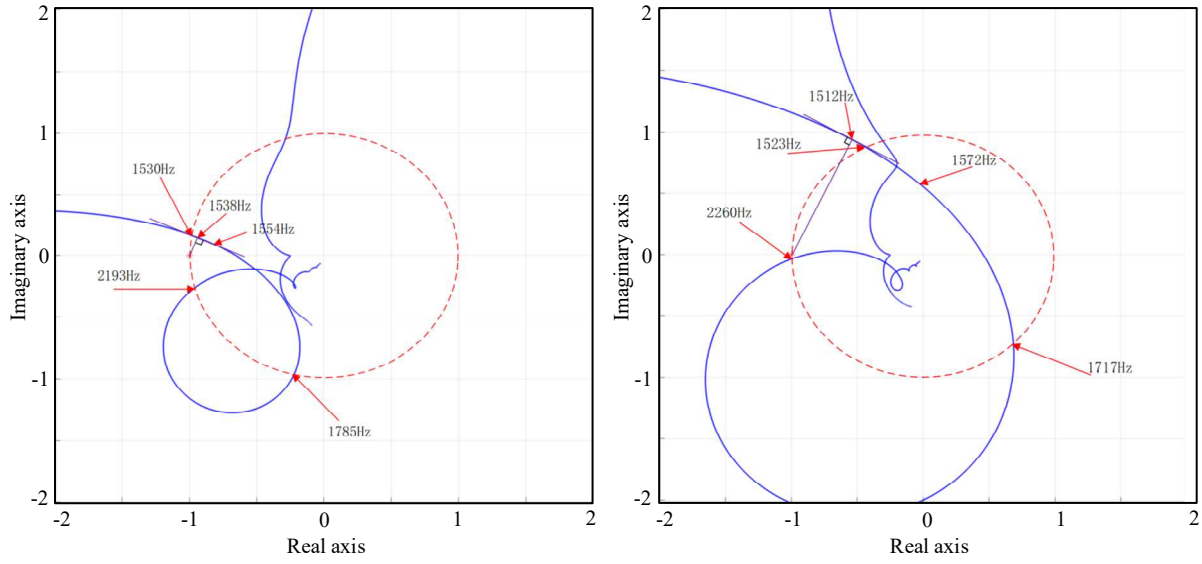

(a) K_p=0.6 K_i=60 (b) K_p=0.8 K_i=80

Fig. 7: Nyquist diagram for the developed impedance model based on DPC

According to the Nyquist diagram in Fig. 7, it can be found that the Nyquist trajectory will pass through the unit circle several times, which is the reason of insufficient phase margin. Apart from that, there will be some errors between FFT results in Fig. 5 and Nyquist diagram in Fig.7. It is caused by the output rotor voltage limitation or PWM limitation. We can modify the impedance model by some describing function when considering these limitations, but these limitations will not influence the cause analysis of resonance issues.

Frequency coupling analysis for DPC and CCC

The simplified model assumes $L_s \approx L_r \approx L_m$ to ignore leakage inductance, and assume $R_g \approx 0$. The influence of PLL can be ignored at high frequency due to limited PLL bandwidth. The $j\omega_g$ and $j\omega_r$ are much smaller than s at high frequency, then the impedance model in Fig. 6 (a) and (b) can be simplified in (6) and (7).

$$\begin{cases} Z_{\mathrm{CCC11}} = Z_{\mathrm{CCC22}} \overset{high\ f}{\approx} \dfrac{s^2 {L_m}^2 \sigma + s L_m K_{pc} e^{-1.5 s/f_s}}{s L_m + K_{pc} e^{-1.5 s/f_s}} \overset{s\to\infty}{\approx} s L_m \sigma + K_{pc} e^{-1.5 s/f_s} \\ Z_{\mathrm{CCC12}} = Z_{\mathrm{CCC21}} \overset{high\ f}{\approx} 0 \end{cases} \tag{6}$$

$$\begin{cases} Z_{\mathrm{DPC11}} = Z_{\mathrm{DPC22}} \overset{high\ f}{\approx} \dfrac{s L_m \sigma + \boldsymbol{U}_{sdq0} K_{pc} e^{-1.5 s/f_s}}{\sigma + 1} \overset{s\to\infty}{\approx} s L_m \sigma + K_{pc} e^{-1.5 s/f_s} \\ Z_{\mathrm{DPC12}} = Z_{\mathrm{DPC21}} \overset{high\ f}{\approx} \dfrac{s L_m \sigma + \boldsymbol{U}_{sdq0} K_{pc} e^{-1.5 s/f_s}}{\boldsymbol{I}_{sdq0} K_{pc} e^{-1.5 s/f_s}} \overset{s\to\infty}{\approx} \dfrac{s L_m \sigma}{\boldsymbol{I}_{sdq0} K_{pc} e^{-1.5 s/f_s}} \end{cases} \tag{7}$$

It can be found that there is no frequency coupling element for CCC, but the DPC has four elements at high frequency. When the s approaches infinity, and consider $\sigma \approx 0$ and $\boldsymbol{U}_{sdq0}=1$, the Z_{CCC11} and Z_{CCC22} have the same form with Z_{DPC11} and Z_{DPC22}. So the most significant difference is that Z_{DPC12} and Z_{DPC21} will not approach to 0 at high frequency, which cause the frequency coupling. The effect of time delay does not decay in frequency coupling element at high frequency, thus the Nyquist trajectory will pass through the unit circle several times in Fig. 7.

In addition, as for inner-current loop and outer-power loop, the time delay will also affect the frequency coupling element when the bandwidth of outer-power loop is large enough.

Conclusion

This paper compares the impedance characteristic of DFIG system between CCC and DPC. From the analysis, it can be found some high-frequency resonance issues under high-frequency capacitive grid when employing DPC. This high-frequency resonance has some interesting phenomenon, such as multiple coupling frequency at high frequency. And this paper analyzes the cause of frequency coupling from DPC, that the time delay in frequency coupling element will deteriorate the stability. In brief, it is not recommended to employ the DPC connected to high-frequency capacitive grid without any impedance shaping methods.

References

[1] B. Hu, H. Nian, M. Li, Y. Xu, Y. Liao and J. Yang, “Impedance-based analysis and stability improvement of DFIG system within PLL bandwidth," *IEEE Trans. Ind. Electron.*, vol. 69, no. 6, pp. 5803-5814, Jun. 2022.

[2] H. Nian, B. Hu, Y. Xu, C. Wu, L. Chen and F. Blaabjerg, “Analysis and reshaping on impedance characteristic of DFIG system based on symmetrical PLL,” *IEEE Trans. Power Electron.*, vol. 35, no. 11, pp. 11720-11730, Nov. 2020.

[3] R. Wang, Q. Sun, W. Hu, Y. Li, D. Ma and P. Wang, “SoC-based droop coefficients stability region analysis of the battery for stand-alone supply systems with constant power loads,” *IEEE Trans. Power Electron.*, vol. 36, no. 7, pp. 7866-7879, Jul. 2021.

[4] C. Zou et al., “Analysis of resonance between a VSC-HVDC converter and the AC Grid,” *IEEE Trans. Power Electron.*, vol. 33, no. 12, pp. 10157-10168, Dec. 2018.

[5] B. Hu, H. Nian, M. Li and Y. Xu, “Impedance characteristic analysis and reshaping method of DFIG system based on DPC without PLL,” *IEEE Trans. Power Electron.*, vol. 68, no. 10, pp. 9767-9777, Oct. 2021.

[6] B. Hu, H. Nian, J. Yang, M. Li and Y. Xu, “High-frequency resonance analysis and reshaping control strategy of DFIG system based on DPC,” *IEEE Trans. Power Electron.*, vol. 36, no. 7, pp. 7810-7819, Jul. 2021.

[7] T. Ohnishi, “Three phase PWM converter/inverter by means of instantaneous active and reactive power control,” *in Proc. Int. Conf. on Ind. Electron*., Nov. 1991, pp. 819–824.

[8] Z. Xie, W. Wu, Y. Chen and W. Gong, “Admittance-based stability comparative analysis of Grid-connected inverters with direct power control and closed-loop current control," *IEEE Trans. Ind. Electron*., vol. 68, no. 9, pp. 8333-8344, Sept. 2021.

[9] B. Hu, H. Nian, M. Li, Y. Liao, J. Yang and H. Tong, “Impedance characteristic analysis and stability improvement method for DFIG system within PLL bandwidth based on different reference frames,” *IEEE Trans. Ind. Electron*., to be published. doi: 10.1109/TIE.2022.3150092.